Asymmetric phase modulation of light with parity-symmetry broken metasurfaces

ELENA MIKHEEVA[1], RÉMI COLOM[1], KARIM ACHOURI[2], ADAM OVERVIG[3], FELIX BINKOWSKI[4], JEAN-YVES DUBOZ[1], SÉBASTIEN CUEFF[5], SHANHUI FAN[6], SVEN BURGER[4,7], ANDREA ALÙ[3,8], PATRICE GENEVET[1,*]

[1]Université Côte d'Azur, CNRS, CRHEA, 06560 Valbonne, France
[2]École Polytechnique Fédérale de Lausanne, Lausanne, VD, Switzerland
[3]Photonics Initiative, Advanced Science Research Center, City University of New York, New York, NY, 10031, USA
[4]Zuse Institute Berlin, Takustraße 7, 14195 Berlin, Germany
[5]Université de Lyon, Institut des Nanotechnologies de Lyon–INL, CNRS UMR 5270 Ecole Centrale de Lyon, Ecully, 69134 France
[6]Department of Electrical Engineering, Stanford University, Stanford, California 94305, USA
[7]JCMwave GmbH, Bolivarallee 22, 14050 Berlin, Germany
[8]Physics Program, Graduate Center, City University of New York, New York, NY, 10016, USA
[*]patrice.genevet@crhea.cnrs.fr

Abstract: Optical components interact with light through radiative channels, and as such they experience intrinsic losses, giving rise to complex-valued eigenfrequencies and singularities. Spatial inversion symmetry breaking -implemented herein by controlling the coupling efficiency between input and output radiative channels of metasurfaces- lifts the directional degeneracy of reflection zeros, and introduces a complex singularity with a positive imaginary part for full 2π-phase modulation of light. Our work establishes a general framework to predict and study the response of resonant systems in photonics and metaoptics.

1. Introduction

Non-Hermicity of photonic and nanophotonic systems provides a powerful framework to engineer innovative light propagation and scattering properties [1–6]. Emerging concepts, such as degenerate eigenstate accumulation and exceptional points at spectral singularities, have recently led to the design of metasurfaces (MSs) with unexpected wavefront modulation capabilities including, among others, polarization decoupling of light, unidirectional transmission, light circular polarizer [7–10]. Beside forming a versatile platform to test topological photonics concepts, MSs have distinct advantages with respect to conventional - refractive - optical components, including planar fabrication, the possibility of multiplexing, and achieving unconventional optical functionalities [11–15]. MSs were demonstrated to be extremely beneficial for various applications such as holography [16–18], LIDAR [19, 20], imaging [21–23], polarization control [24, 25], quantum state detection [26], etc.

The design of metasurfaces requires full $2\pi-$phase modulation, which is generally realized by leveraging several phase-control mechanisms, including the resonant interaction of light with nanoscale dielectric or metallic particles. The common approach to the design of resonant phase MSs relies on the well-known property that scattering of structures supporting a single resonant mode provides a maximum phase shift of π with respect to the incoming wavefront [27]. This limited phase modulation occurs when the photonic system is time-reversal-symmetric in transmission, or both parity- and time-reversal-symmetric in reflection [28–30]. To extend the coverage to the required full 2π response, the phase is often "doubled" by adding a back reflector, or combining two modes by geometric parameter tuning [31]. This idea of doubling the phase using multiple resonances has ensued from oversimplified models that do not consider the interaction of resonantly scattered light with a non-resonant background, that is the intrinsic non-Hermicity of the system. Taking these interference effects into consideration and looking at this problem using theoretical concepts associated with non-Hermitian physics provide insights into the mechanism of light scattering by nanostructured interfaces.

Here, we present physical insights and design guidelines associated with the topological properties of metasurfaces to unify the design principles of resonant phase components and to further achieve asymmetric phase modulation in reflection. We rely on complex-frequency analysis to draw conclusions on the physics of metasurfaces and guide the designs towards the engineering of innovative nanophotonic devices [28]. By studying the analytical formulas associated with the complex values of the reflection poles and zeros, we are able to express the interplay between absorption loss, scattering loss, and scattering gain leading to zero and pole separation. In particular, we show that the total effective gain in the system should prevail over the total effective loss to fulfill this condition. We illustrate these analytical results with simple metal-dielectric-metal structures previously proposed in the literature and further exploit them to design interfaces featuring extremely high coupling asymmetry between two channels. More precisely, we link the asymmetric response with the absence of z-inversion symmetry across the interface, and numerically demonstrate this behavior using vertically-asymmetric nanostructures composed of conically-shaped nanophotonic building blocks. Our description establishes a clear connection between phase-controlling metasurfaces and the class of metasurfaces supporting phase singularities [7, 31–36]. Our results bring us to the general conclusion that any resonant phase metasurface that operates over a full phase range in reflection or transmission requires proper engineering of the position of topological singularities in the complex frequency plane.

2. Results and discussions

2.1. A necessary condition for the 2π resonant phase gradient

Coupling of the metasurface to the surrounding environment can be described via linear operators supporting complex-valued eigenfrequencies, which express the non-Hermicity of the system. The imaginary parts of these eigenfrequencies essentially describe the rate of energy exchange between the resonators and the environment. The physical quantities representing the responses of these components, including reflection or transmission coefficients, as well as any other response function of the linear systems, can be expanded in the complex plane according to the Weierstrass factorization theorem [37–47] as

$$\det(r) \sim \prod_m \frac{\omega - \omega_{\mathrm{RZ,m}}}{\omega - \omega_{\mathrm{P,m}}} \tag{1}$$

This expression contains an infinite number of singular points (poles and zeros) related to the eigenvalues of the system. As an example, poles correspond to eigen-solutions with purely outgoing fields. Reflection zeros instead describe purely incoming waves in one set of channels and outgoing light exiting the device only through the complementary set of channels [47, 48]. [1] When we are operating a photonic system over a limited frequency range, its response is dominated by one or just a few zero-pole pairs. The contribution of the other factors can be truncated and simply lumped together leading to non-resonant background. Zeros and poles are phase singularities with opposite handedness, which are connected by a branch cut - a phase jump appearing due to the ambiguous value of the phase. We have previously shown that a sufficient condition for an optical component to realize a full 2π resonant phase shift is to have at least one zero-pole pair separated by the real axis [28]. The branch cut crossing

[1]Note that for light scattering, poles and zeros are often calculated for the scattering matrix, but they also appear for reflection or transmission matrices. While poles of scattering, reflection, and transmission matrices always coincide, the zeros are generally all different.

confirms previous numerical calculations [49] and further unifies all resonant phase modulation mechanisms under a simple condition on the positions of complex singularities. Considering the time-convention $e^{-i\omega t}$, poles are bound to have a negative imaginary part in passive systems which results in avoiding energy divergence due to causality [50]. Fulfilling the branch cut crossing condition thus requires engineering the zero positions to have a positive imaginary part. For metasurfaces operating in reflection, analytical expressions for the positions of complex zeros and poles can be calculated using temporal coupled modes theory (TCMT). [47, 48, 51, 52] TCMT has been previously applied to study, among others, the asymmetric response of photonic structures. [53–55] The description of a metasurface operating at normal incidence can be represented with the TCMT as a two-port system supporting only one dominant resonance in the frequency range of interest. Complex reflection zeros ω_{RZ} (Eq. 2a) and poles ω_P (Eq. 2b) are expressed as:

$$\omega_{\mathrm{RZ}} = \omega_0 - i\gamma_0 + i\gamma_1 - i\gamma_2 \tag{2a}$$

$$\omega_{\mathrm{P}} = \omega_0 - i\gamma_0 - i\gamma_1 - i\gamma_2 \tag{2b}$$

where γ_0, γ_1, and γ_2 represent the absorption loss, coupling to the first (top) and second (bottom) channels respectively. Note that in a case of an active medium, this equation will contain an additional term entering with a plus sign and representing gain. In this description, ω_0 is the real eigenfrequency of the structure as if the structure were not interacting with the environment. Details on the derivations are presented in the Supplementary Material. The equation (Eq. 2a) contains all information needed to predict the branch cut crossing condition to achieve a full 2π resonant phase response, that is for $\mathrm{Im}(\omega_{\mathrm{RZ}}) > 0$. In other words, if the illumination comes from the first channel, coupling to it should be larger than the sum of the coupling to the second channel (that can be considered as an effective loss) and absorption loss. This regime is described in the literature as the "overcoupling" regime [56] [2]. The other possible situations are "critical coupling" ($\mathrm{Im}(\omega_{\mathrm{RZ}}) = 0$) and "undercoupling" ($\mathrm{Im}(\omega_{\mathrm{RZ}}) < 0$) regimes. For the latter two cases, resonant 2π phase retardation is not achievable at normal incidence. Our first conclusion is that resonant metasurfaces operating in reflection achieve full phase modulation when operating in the overcoupling regime, corresponding to the separation by the real frequency axis of an isolated complex-valued zero-pole pair.

We identified another critical condition to split the zero and pole of a pair in the complex plane: the zeros can be manipulated to be placed in the upper part of the complex plane whenever the system suffers from either absorption losses or when it presents some sort of asymmetry. Suppose we are considering a perfectly symmetric and lossless system. The absence of loss and gain implies that the system verifies time-inversion symmetry (T- symmetry). The z-inversion symmetry (P- parity) is also verified so that the system is both P- and T-symmetric. Because of the out-of-plane inversion symmetry of the structure, the reflection zeros of the system, illuminated from the top have the same complex frequency as the zeros of the system illuminated from the bottom. The time-reversal symmetry also imposes that these two "bi-directional" zeros are complex conjugates. The only solution is thus that the zeros are either all real or exist in pairs with complex conjugate values. If we consider that the response of both P- and T-symmetric systems in a restricted spectral region of interest is dominated by only one resonance, we immediately conclude that the reflection zeros, whether the system is excited from the top or from the bottom, are identical and for this reason, have to be real $\omega'_{\mathrm{RZ}} = \omega^*_{\mathrm{RZ}} \in \mathbb{R}$, as schematically represented in Fig. 1a. These very specific cases have been identified as reflectionless scattering modes (R-zeros on the real axis) for both direct and time-reversed propagation [47]. As the parity symmetry is broken, for example by considering different sub- and superstrate, the zeros of the reflection can

[2] In TCMT this term can be used for total radiative coupling prevailing over absorption loss. Here we used it by considering that radiative coupling to the second channel (in this case, transmission channel) could also be associated with a loss for a first (reflection) channel

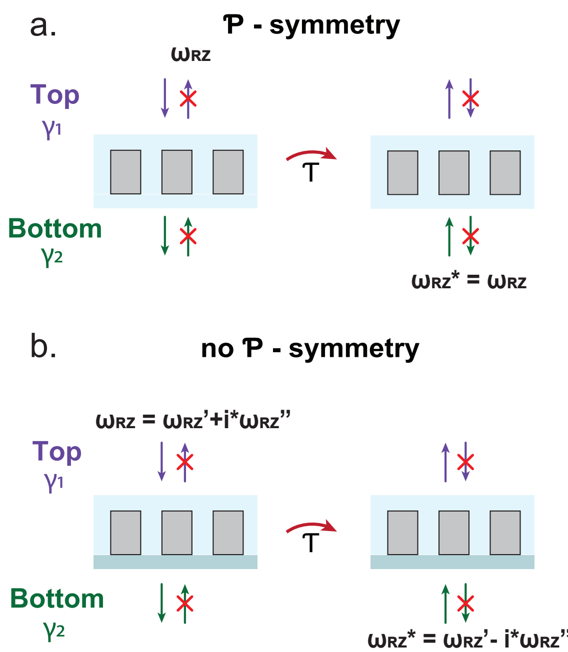

Fig. 1. a. Schematic representation of the time-reversal operator to parity-symmetric and asymmetric metasurfaces. The structures considered are made of non-absorbing and non-amplifying material. This way, the application of time-reversal symmetry on the system, that is imposing the condition $T : t \longrightarrow -t$, results in both inverting input to output boundary conditions and imposing complex conjugated values on the zeros frequencies. On top, the reflection zeros associated with light impinging onto the metasurface from both directions are bound to the real axis. On the bottom, the structure geometry is specifically chosen to break the z-inversion symmetry. Note that in this latter case, time-reversal symmetry imposes the reflection zeros to be complex conjugated.

be different for top and bottom incidence, meaning that these zeros are not forced to stay on the real frequency axis. However, they remain complex conjugates of each other in the case of a lossless system after applying time-reversal symmetry, which imposes that $\omega'_{RZ} = \omega^*_{RZ} \in \mathbb{C}$, see Fig. 1b). Similarly, breaking time-reversal symmetry by adding losses or gain, even for a symmetric system, is also a sufficient condition to move the zeros from the real frequency axis. Note, however, that if the system is neither P- nor T- symmetric while preserving the overall PT-symmetry, zeros are expected to be bound to the real axis.

2.2. Controlling the position of reflection phase singularities of asymmetric metal-insulator-metal metastructures

Placing a mirror with close to unity reflection at the bottom of the structure is the most straightforward and the most employed way of breaking simultaneously z-inversion and time-reversal symmetries. Indeed, metallic features can not only cancel the transmission of light but also bring unavoidable optical losses[3]. As stipulated in the introduction, we can leverage both effects to control the complex frequencies of top and bottom reflection zero singularities. We

[3] here time-reversal symmetry is broken because of the losses but it doesn't mean that the system becomes nonreciprocal.

already know from previous works that tuning geometrical parameters of a structure changes the absorption γ_0 and the coupling coefficients γ_1 and γ_2 and that full phase modulation can be harvested by circulating around a zero amplitude of the reflection coefficient [31–34, 57, 58]. In these papers, phase, and amplitude color-coded simulation maps, calculated by varying both the structural parameters and the real frequency of excitation, indicated the presence of a zero of reflectivity and full phase modulation. It has been shown that this condition is guaranteed when radiative losses into the reflection channel prevail over absorption losses [31]. A similar idea of circulation has been recently proposed in the context of zeros of polarization conversion near exceptional points [7]. In the following, we analyzed this problem from the non-Hermitian perspective. Scattering problems driven by light sources with complex-valued frequencies are solved using the finite-element-based software package JCMsuite. We then prove that the complex singularities observed in these systems occur at the transition when a zero and pole of a pair become separated by the real frequency axis. For a system including a thick metallic bottom mirror, we can conveniently set the coupling to the transmission channel to $\gamma_2 = 0$. Thus, the expressions for the imaginary parts of the reflection zeros and poles (calculated analogously from Eqs. (2a) and (2b)) contain only two terms: $\mathrm{Im}(\omega_{\mathrm{RZ}}) = \gamma_1 - \gamma_0$, $\mathrm{Im}(\omega_{\mathrm{P}}) = -\gamma_1 - \gamma_0$. From this system of equations, and numerically calculating the imaginary parts of poles and zeros, we can evaluate the absorption loss γ_0 and the coupling coefficient γ_1: $\gamma_1 = \frac{|\mathrm{Im}(\omega_{\mathrm{P}})| + \mathrm{Im}(\omega_{\mathrm{RZ}})}{2}$ and $\gamma_0 = \frac{|\mathrm{Im}(\omega_{\mathrm{P}})| - \mathrm{Im}(\omega_{\mathrm{RZ}})}{2}$. We apply this analysis to the example discussed in [58]. The structure studied in the latter article is a typical example of a MIM-metasurface consisting of a gold mirror, glass spacer of variable thickness d, and another thin gold layer nanostructured into rectangular antennas (Fig. 2a). To reproduce the results, we adopted the same parameters, i.e. a reflectivity of the bottom mirror $r_m = 1$, the refractive index of a spacer $n = 1.5$, lattice pitch $a = 350$ nm and the parameters of the gold antennas exactly as in the former article. We first reproduced the same reflection amplitude and phase maps as a function of real frequency and the spacer thickness d (Fig. 2b,c), consistently with Fig. 2c in [58]. At first glance, both reflection maps seem to reveal pairs of reflection zeros appearing for a specific range of spacer thickness. In the latter reference, these zeros were attributed to a pair of topological singularities with opposite charge ± 1. Here we apply the complex frequency analysis to this problem, that is we compute the response of the system using a higher-order finite element method, called JCMsuite solver [59], assuming continuation of Maxwell equations in the complex frequency plane by considering a complex-frequency excitation. We could then formally identify the role played by complex singularities. We first calculate the reflection amplitude and phase for a given spacer thickness of $d = 130$ nm (corresponding to one reflection zero in Fig. 2b) assuming complex excitation frequency and extract the associated real frequency response (Fig. 2d). Complex frequency reveals topological singularities, the expected pole and zero of reflection, represented on the complex frequency amplitude map respectively by a maximum and a minimum of reflection amplitude. The phase map shows that each of these features is surrounded, as previously discussed, by topological 2π clockwise and anticlockwise phase vortices (± 1) [28]. The complex plane analysis thus reveals that for this specific geometrical parameters, pole and zero are separated by the real axis and that a 2π resonant phase modulation is obtained by varying the frequency along the real axis. The position of the zero in the vicinity of the real axis also leads to a decreased reflection amplitude resulting in a dip of the reflection coefficient for real frequency excitation. We also calculated both real- and complex- frequency dependent reflection for another spacer thickness of $d = 250$ nm (Fig. 2e) and we did not observe any significant resonant spectral responses, neither in phase nor in amplitude. Complex plane reveals that both singularities are located in a lower frequency plane, each positioned sufficiently far away from the real axis to significantly influence the response of the system at real frequency.

The complex frequency analysis is further employed to follow the detailed evolution of the positions of zero and pole singularities as a function of the spacer thickness. The full evolution is presented in a video in Supplemental material (Complex_plane_d10-550nm.avi, Complex_plane_d270-275nm.avi). We observe that both zero and pole singularities move in circles, repeating similar trajectories with the periodicity related to the Fabry-Perot modes. We observe that the points of zero reflection amplitude, which were apparently identified previously as real space phase singularities, in Fig. 2b,c, correspond in fact to the same complex reflection zero ω_{RZ} crossing the real axis twice, moving back and forth between the lower and the upper part of the complex plane (Fig. 2f). Note that whenever the zero crosses the real frequency axis, the system reaches the critical coupling condition ($\gamma_0 = \gamma_1$) leading to perfect absorption [10]. This observation helps us understand that if indeed topological singularities of the opposite charge -the poles and the zeros- govern the optical response of this structure, they do not appear in the real parameters space, but in the complex frequency space. Moreover, our analysis brings us to the conclusion that only one zero is responsible for the observation of effective singularities previously appearing in the real parameters space. Tracking the complex values as a function of d also enables us to identify parameter regions where a zero-pole pair is separated by a real axis, that is the parameter regions where a 2π phase accumulation as a function of real-frequency can be achieved (see the gray shaded regions in Fig. 2f).

To complete our analysis, we obtained the complex values of the poles and zeros and used this information to calculate the coupling coefficient to the reflection channel γ_1 and the absorption losses γ_0. The results presented in Fig. 2g confirm that in the 2π resonant phase shift regions, the coupling to the reflection channel prevails over absorption, i.e. $\gamma_1 > \gamma_0$, confirming the earlier results on the existence of reflection zeros in the real parameters space [6, 7, 60–63].

2.3. Asymmetric response of dielectric cones structure

In the following, we propose to further leverage our understanding of symmetry arguments to achieve a physical response similar to MIM structures but using dielectric nanostructures, i.e. nanostructures composed of a material having a real refractive index. As time-reversal symmetry still holds, reflection zeros in the direct (illumination from the top) and time-reversed (illumination from the bottom) scenarios are complex-conjugated. If the system is also P-symmetric, direct and time-reversed reflection zeros are forced to coincide [4]. As discussed previously, breaking the parity symmetry relaxes the second requirement and allows zeros to become complex. In our study, we now consider a simple lossless ($\gamma_0 = 0$) silicon-based metasurface ($n = 3.5$) presenting broken out-of-plane symmetry, realized by truncating pillar structures to form cones. The structure height is fixed in the rest of the analysis to $h = 600$ nm (Fig. 3a). Pillars are arranged in a 2D square lattice with a fixed period of $p = 800$ nm. We also embed the interface into a homogeneous medium with a refractive index $n = 1.5$. When the pillar shape is preserved, i.e. when their top and bottom diameters defined as L_1 and L_2 respectively are equal ($L_1 = L_2$), this structure is completely symmetric in all directions, indicating that the system remains identical upon z-inversion (and parity) symmetry. The reflection zeros associated with the parity-symmetric system are thus identical and real, whether the system is excited from the top or from the bottom. Indeed for lossless metasurface, $\gamma_0 = 0$ and its coupling coefficient to substrate and superstrate are identical, so that in the Eq. 2a, $\gamma_1 = \gamma_2$, leading to $\mathrm{Im}(\omega_{RZ}) = 0$. [5] However, when the coupling asymmetry is introduced by varying the top diameter L_1 between 400 nm and 500 nm and leaving the bottom diameter at $L_2 = 500$ nm, the structure is no longer preserved under the parity operation. Breaking z-inversion thus moves the zeros to the complex plane. To characterize and compare the behavior of the system upon the top and bottom illumination, we

[4]Note that flipping upside down the structure and exchanging the boundary conditions with respect to the xy-plane at $z = 0$ implies breaking P-symmetry [47]

[5]We note that, with respect to the reflection case, the coupling coefficients γ_1 and γ_2 do not have such a similar straightforward influence on the positions of the transmission zeros. Transmission zeros are bound to the real axis only by the time-reversal symmetry of the structure. This point, which extends beyond the scope of this manuscript, is further discussed in more detail in the Supplementary Material.

computed both top and bottom reflection coefficients using finite element method simulations for the asymmetric case $L_1/L_2 = 0.84$ and compared their amplitude and phase responses. The results are presented in Fig. 3 b and c. We observe that for this specific value of the asymmetry, the metasurface behaves similarly as an efficient mirror with almost unity reflection over the entire spectral region for both illumination directions. However, the phase behavior is extremely asymmetric, showing a drastic resonant 2π phase variation for light impinging from the top, with only a linear dispersion -characteristic of the propagation phase across the simulation volume- is observed using bottom excitation.

We also link the asymmetric phase variation observed in Fig. 3 b. and c. with the position of zero singularities in the complex plane. We thus compute both top and bottom reflection cases for the asymmetric structure in the complex frequency plane using JCMsuite. In both illumination cases, i.e. considering top and bottom light impinging on the structure from the thin or the wide section of the cone respectively, we observe that the complex plane optical response is always composed of only one zero-pole pair. Fig. 3d. and e. shows the evolution of the pole and the zero as the structure is changing from symmetric to asymmetric (L_1/L_2 is changing from 1 to 0.8). For the symmetric case with $L_1/L_2 = 1$, the structure is P-symmetric and the reflection zeros are bound to the real axis ($\omega'_{\mathrm{RZ}} = \omega^*_{\mathrm{RZ}} = \omega_{\mathrm{RZ}}$). Increasing the asymmetry gradually moves away ω_{RZ} and ω'_{RZ} from the real axis in the opposite complex half-planes. For the geometric asymmetry leading to maximally asymmetric response, i.e. when $L_1/L_2 = 0.84$, we observe that the top illumination condition achieves almost unity reflection and full phase modulation. This condition is characterized by a complex zero frequency that is reaching the conjugated value of its pole ($\omega_{\mathrm{RZ}} \approx \omega^*_{\mathrm{P}}$). Similar complex conjugation between pole and zero has recently been shown to achieve extremely high modulation efficiency [64]. In comparison, the bottom illumination case does not provide extensive phase modulation simply because the associated zero, which due to time-reversal symmetry consideration is conjugated to the top illumination zero, has a large imaginary part and, as such, does not influence the real frequency response of the metasurface (Fig. 3c.).

At this point, we recall the TCMT analytical expressions for reflection poles and zeros, considering here a lossless system with two-ports, i.e. $\gamma_0 = 0$ in Eqs. 2a, 2b, and simplify the expressions to calculate the coupling coefficients γ_1 and γ_2, we obtain

$$\begin{cases} \gamma_1 = \frac{|\mathrm{Im}(\omega_{\mathrm{P}})|+\mathrm{Im}(\omega_{\mathrm{RZ}})}{2} \\ \gamma_2 = \frac{|\mathrm{Im}(\omega_{\mathrm{P}})|-\mathrm{Im}(\omega_{\mathrm{RZ}})}{2} \end{cases} \tag{3}$$

With these equations and after numerically obtaining $\mathrm{Im}(\omega_{\mathrm{RZ}})$, $\mathrm{Im}(\omega_{\mathrm{P}})$, we calculate the coupling coefficients γ_1 and γ_2. We observe that the coupling to the reflection channel γ_1 increases with asymmetry, while γ_2 decreases with asymmetry to reach 0 for $L_1/L_2 = 0.84$, as shown in Fig. 3f. We show how the reflection phase and amplitude are changing with a gradual increase of asymmetry in the case of top illumination in Supplementary information. We also calculate the minimum reflection R_{min} in a considered frequency region as a function of diameters ratio (L_1/L_2). These data, shown on the same plot in Fig. 3g., are presented as a function of the coupling asymmetry γ_2/γ_1. Increasing the coupling asymmetry (γ_1/γ_2 decreases) significantly increases the reflection efficiency of the metasurface over the spectral region of interest. This condition creates a unique situation, similar to a Gires-Tournois resonator with approximately unity reflection, but with one layer of dielectric only and without using a metallic or Bragg mirror (Fig. 1b.). The reflection tends to unity for both bottom and top illumination. However, due to the complex conjugation of top and bottom zeros in a time-reversal symmetric system, we obtain an asymmetric phase modulation, characterized by a single-side resonant phase modulation of interest for the design of metasurfaces. Again, this behavior is shown to be connected to the presence of a zero in the upper part of the complex-frequency plane.

3. Conclusion

In conclusion, we provide guidelines to achieve full-phase modulation as a function of the real frequency in reflection. Our analysis reveals that bringing the reflection zeros to the upper part of the complex plane, a condition previously identified as a sufficient condition for full 2π phase modulation can be realized using nanostructured interfaces that break the z-inversion symmetry. Breaking the out-of-plane symmetry allows reaching a full phase modulation with only one resonant mode which is less sensitive to parameter change than the careful adjustment of the interaction between two scattering modes usually proposed for Huygens metasurfaces. Instead, we show that any array of nanostructures that behaves as a Gires-Tournois resonator can feature narrow-band high reflection efficiency and full-phase modulation for an extended stretch of parameter values. This approach could thus have a high impact on the emerging field of non-local metasurfaces employing high quality factor resonant mode. [27,65–67]. Our work unifies, via the analysis of complex frequency position of reflection singularities, the physics of the overwhelming majority of MIM phase-gradient metasurfaces operating in reflection [6,7,57,58,60–63]. We also rely on a temporal coupled-mode theory to study the positions of the complex topological singularities and to generalize the previously defined overcoupling regime associated with the full-phase modulation regime. This regime is characterized by the condition at which the coupling to the reflection channel exceeds the sum of the coupling to the transmission channel and the absorption loss. Linking these quantities with the imaginary parts of complex poles and zeros characterizing resonant reflection brings new physical insights to the problem of 2π phase modulation. Additionally, the realization of a strong asymmetric phase response between forward and backward reflection with z-inversion symmetry broken surfaces further highlights the interest in considering topological singularities in the complex plane to design metasurfaces in general. Incidentally, direct excitation of these complex zeros using non-monochromatic light enables extreme scattering responses, which are no longer limited by conventional physical limits such as causality, passivity, and conservation of energy [68], and as such, extensive developments associated with complex singularities are expected in the coming years.

See Supplemental Material for the detailed derivations of equations with temporal coupled mode theory, simulation of silicon cones metasurface response in a wider parameters range, a video demonstrating the evolution of complex poles and zeros in metal-insulator-metal structure as the spacer thickness varies from 10 *nm* to 550 *nm*, a second video showing an evolution of the same zero-pole pair in the zoomed region in the lower part of the complex plane in a reduced range of spacer thickness variation (from 250 *nm* to 275 *nm*).

4. Acknowledgments

P.G. acknowledges financial support by the French National Research Agency ANR Project DILEMMA (ANR-20-CE09-0027). S.C., P.G. and E.M. acknowledge financial support by the French National Research Agency ANR Project Meta-On-Demand (ANR-20-CE24-0013). P.G. and R.C. acknowledges support from the European Innovation Council (EIC) project TwistedNano (under the grant agreement number Pathfinder Open 2021- 101046424). J.Y.D. and P.G. acknowledges financial support by the French National Research Agency ANR SWEET (ANR-22-CE24-0005). K.A. gratefully acknowledges funding from the Swiss National Science Foundation (project PZ00P2_193221). S.F. acknowledge the support of a U. S. AFORS MURI project (Grant No. FA9550-21-1-0312). A.A. and A.O. were supported by the Simons Foundation and the Air Force Office of Scientific Research.

References

1. S. Dong, G. Hu, Q. Wang, Y. Jia, Q. Zhang, G. Cao, J. Wang, S. Chen, D. Fan, W. Jiang, Y. Li, A. Alù, and C.-W. Qiu, "Loss-Assisted Metasurface at an Exceptional Point," ACS Photonics **7**, 3321–3327 (2020).

2. M. Liu, C. Zhao, Y. Zeng, Y. Chen, C. Zhao, and C.-W. Qiu, "Evolution and Nonreciprocity of Loss-Induced Topological Phase Singularity Pairs," Phys. Rev. Lett. **127**, 266101 (2021).
3. D. G. Baranov, A. Krasnok, and A. Alu, "Coherent virtual absorption based on complex zero excitation for ideal light capturing," Optica **4**, 1457 (2017).
4. Z. Sakotic, A. Krasnok, A. Alu, and N. Jankovic, "Topological scattering singularities and embedded eigenstates for polarization control and sensing applications," Photonics Res. **9**, 1310 (2021).
5. X. Gu, R. Bai, C. Zhang, X. R. Jin, Y. Q. Zhang, S. Zhang, and Y. P. Lee, "Unidirectional reflectionless propagation in a non-ideal parity-time metasurface based on far field coupling," Opt. Express **25**, 11778 (2017).
6. M. Kang, H.-X. Cui, T.-F. Li, J. Chen, W. Zhu, and M. Premaratne, "Unidirectional phase singularity in ultrathin metamaterials at exceptional points," Phys. Rev. A **89**, 065801 (2014). Publisher: American Physical Society.
7. Q. Song, M. Odeh, J. Zúñiga-Pérez, B. Kanté, and P. Genevet, "Plasmonic topological metasurface by encircling an exceptional point," Science **373**, 1133–1137 (2021). Publisher: American Association for the Advancement of Science.
8. Z. Deng, F. Li, H. Li, X. Li, and A. Alu, "Extreme Diffraction Control in Metagratings Leveraging Bound States in the Continuum and Exceptional Points," Laser & Photonics Rev. p. 2100617 (2022).
9. S. K. Ozdemir, S. Rotter, F. Nori, and L. Yang, "Parity–time symmetry and exceptional points in photonics," Nat. Mater. **18**, 783–798 (2019).
10. W. R. Sweeney, C. W. Hsu, S. Rotter, and A. D. Stone, "Perfectly Absorbing Exceptional Points and Chiral Absorbers," Phys. Rev. Lett. **122**, 093901 (2019).
11. N. Yu, P. Genevet, M. A. Kats, F. Aieta, J.-P. Tetienne, F. Capasso, and Z. Gaburro, "Light Propagation with Phase Discontinuities: Generalized Laws of Reflection and Refraction," Science **334**, 333–337 (2011).
12. P. Genevet, F. Capasso, F. Aieta, M. Khorasaninejad, and R. Devlin, "Recent advances in planar optics: from plasmonic to dielectric metasurfaces," Optica **4**, 139–152 (2017).
13. Y.-Y. Xie, P.-N. Ni, Q.-H. Wang, Q. Kan, G. Briere, P.-P. Chen, Z.-Z. Zhao, A. Delga, H.-R. Ren, H.-D. Chen, C. Xu, and P. Genevet, "Metasurface-integrated vertical cavity surface-emitting lasers for programmable directional lasing emissions," Nat. Nanotechnol. **15**, 125–130 (2020).
14. N. A. Rubin, G. D'Aversa, P. Chevalier, Z. Shi, W. T. Chen, and F. Capasso, "Matrix Fourier optics enables a compact full-Stokes polarization camera," Science **365**, eaax1839 (2019).
15. E. Arbabi, S. M. Kamali, A. Arbabi, and A. Faraon, "Full-Stokes Imaging Polarimetry Using Dielectric Metasurfaces," ACS Photonics **5**, 3132–3140 (2018).
16. G. Zheng, H. Mühlenbernd, M. Kenney, G. Li, T. Zentgraf, and S. Zhang, "Metasurface holograms reaching 80% efficiency," Nat. Nanotechnol. **10**, 308–312 (2015).
17. Y. Hu, X. Luo, Y. Chen, Q. Liu, X. Li, Y. Wang, N. Liu, and H. Duan, "3D-Integrated metasurfaces for full-colour holography," Light. Sci. & Appl. **8**, 86 (2019).
18. Q. Song, X. Liu, C.-W. Qiu, and P. Genevet, "Vectorial metasurface holography," Appl. Phys. Rev. **9**, 011311 (2022). Publisher: American Institute of Physics.
19. R. Juliano Martins, E. Marinov, M. A. B. Youssef, C. Kyrou, M. Joubert, C. Colmagro, V. Gâté, C. Turbil, P.-M. Coulon, D. Turover, S. Khadir, M. Giudici, C. Klitis, M. Sorel, and P. Genevet, "Metasurface-enhanced light detection and ranging technology," Nat. Commun. **13**, 5724 (2022).
20. J. Park, B. G. Jeong, S. I. Kim, D. Lee, J. Kim, C. Shin, C. B. Lee, T. Otsuka, J. Kyoung, S. Kim, K.-Y. Yang, Y.-Y. Park, J. Lee, I. Hwang, J. Jang, S. H. Song, M. L. Brongersma, K. Ha, S.-W. Hwang, H. Choo, and B. L. Choi, "All-solid-state spatial light modulator with independent phase and amplitude control for three-dimensional LiDAR applications," Nat. Nanotechnol. **16**, 69–76 (2021).
21. R. Sawant, D. Andrén, R. J. Martins, S. Khadir, R. Verre, M. Käll, and P. Genevet, "Aberration-corrected large-scale hybrid metalenses," Optica **8**, 1405–1411 (2021).
22. H. Kwon, E. Arbabi, S. M. Kamali, M. Faraji-Dana, and A. Faraon, "Single-shot quantitative phase gradient microscopy using a system of multifunctional metasurfaces," Nat. Photonics **14**, 109–114 (2020).
23. M. Bosch, M. R. Shcherbakov, K. Won, H.-S. Lee, Y. Kim, and G. Shvets, "Electrically Actuated Varifocal Lens Based on Liquid-Crystal-Embedded Dielectric Metasurfaces," Nano Lett. **21**, 3849–3856 (2021).
24. Q. Song, S. Khadir, S. Vézian, B. Damilano, P. D. Mierry, S. Chenot, V. Brandli, and P. Genevet, "Bandwidth-unlimited polarization-maintaining metasurfaces," Sci. Adv. **7**, eabe1112 (2021). Publisher: American Association for the Advancement of Science.
25. Q. Song, A. Baroni, P. C. Wu, S. Chenot, V. Brandli, S. Vézian, B. Damilano, P. de Mierry, S. Khadir, P. Ferrand, and P. Genevet, "Broadband decoupling of intensity and polarization with vectorial Fourier metasurfaces," Nat. Commun. **12**, 3631 (2021).
26. Z. Gao, Z. Su, Q. Song, P. Genevet, and K. E. Dorfman, "Metasurface for complete measurement of polarization Bell state," Nanophotonics (2022). Publisher: De Gruyter.
27. K. Shastri and F. Monticone, "Nonlocal flat optics," Nat. Photonics **17**, 36–47 (2023).
28. R. Colom, E. Mikheeva, K. Achouri, J. Zuniga-Perez, N. Bonod, O. J. F. Martin, S. Burger, and P. Genevet, "Crossing of the Branch Cut: The Topological Origin of a Universal 2π-Phase Retardation in Non-Hermitian Metasurfaces," Laser & Photonics Rev. p. 2200976 (2023).
29. H. Kwon, T. Zheng, and A. Faraon, "Nano-electromechanical spatial light modulator enabled by asymmetric resonant dielectric metasurfaces," Nat. Commun. **13**, 5811 (2022).

30. A.-S. B.-B. Dhia, L. Chesnel, and V. Pagneux, “Trapped modes and reflectionless modes as eigenfunctions of the same spectral problem,” Proc. Royal Soc. A: Math. Phys. Eng. Sci. **474**, 20180050 (2018).
31. J. Y. Kim, J. Park, G. R. Holdman, J. T. Heiden, S. Kim, V. W. Brar, and M. S. Jang, “Full 2π tunable phase modulation using avoided crossing of resonances,” Nat. Commun. **13**, 2103 (2022).
32. S. Han, S. Kim, S. Kim, T. Low, V. W. Brar, and M. S. Jang, “Complete Complex Amplitude Modulation with Electronically Tunable Graphene Plasmonic Metamolecules,” ACS Nano **14**, 1166–1175 (2020).
33. R. Sabri and H. Mosallaei, “Inverse design of perimeter-controlled InAs-assisted metasurface for two-dimensional dynamic beam steering,” Nanophotonics **11**, 4515–4530 (2022).
34. D. B. Haim, L. Michaeli, O. Avayu, and T. Ellenbogen, “Tuning the phase and amplitude response of plasmonic metasurface etalons,” Opt. Express **28**, 17923 (2020).
35. L. Chen, S. M. Anlage, and Y. V. Fyodorov, “Statistics of Complex Wigner Time Delays as a Counter of S-Matrix Poles: Theory and Experiment,” Phys. Rev. Lett. **127**, 204101 (2021).
36. L. Chen and S. M. Anlage, “Use of transmission and reflection complex time delays to reveal scattering matrix poles and zeros: Example of the ring graph,” Phys. Rev. E **105**, 054210 (2022).
37. M. C. Hutley and D. Maystre, “The total absorption of light by a diffraction grating,” Opt. Commun. **19**, 431–436 (1976).
38. R. A. Depine, V. L. Brudny, and J. M. Simon, “Phase behavior near total absorption by a metallic grating,” Opt. Lett. **12**, 143–145 (1987).
39. M. Nevière, R. Reinisch, and E. Popov, “Electromagnetic resonances in linear and nonlinear optics: phenomenological study of grating behavior through the poles and zeros of the scattering operator,” J. Opt. Soc. Am. A **12**, 513 (1995).
40. R. Petit, ed., *Electromagnetic Theory of Gratings* (Springer, Berlin, Heidelberg, 2011), softcover reprint of the original 1st ed. 1980 edition ed.
41. D. Maystre, “Theory of Wood’s Anomalies,” in *Plasmonics,* vol. 167 S. Enoch and N. Bonod, eds. (Springer Berlin Heidelberg, Berlin, Heidelberg, 2012), pp. 39–83.
42. D. Maystre, “Diffraction gratings: An amazing phenomenon,” Comptes Rendus Physique **14**, 381–392 (2013).
43. V. Grigoriev, S. Varault, G. Boudarham, B. Stout, J. Wenger, and N. Bonod, “Singular analysis of Fano resonances in plasmonic nanostructures,” Phys. Rev. A **88**, 063805 (2013).
44. V. Grigoriev, A. Tahri, S. Varault, B. Rolly, B. Stout, J. Wenger, and N. Bonod, “Optimization of resonant effects in nanostructures via Weierstrass factorization,” Phys. Rev. A **88**, 011803 (2013).
45. F. Alpeggiani, N. Parappurath, E. Verhagen, and L. Kuipers, “Quasinormal-Mode Expansion of the Scattering Matrix,” Phys. Rev. X **7**, 021035 (2017).
46. A. Krasnok, D. Baranov, H. Li, M.-A. Miri, F. Monticone, and A. Alú, “Anomalies in light scattering,” Adv. Opt. Photonics **11**, 892 (2019).
47. W. R. Sweeney, C. W. Hsu, and A. D. Stone, “Theory of reflectionless scattering modes,” Phys. Rev. A **102**, 063511 (2020). Publisher: American Physical Society.
48. W. R. Sweeney, “Electromagnetic Eigenvalue Problems and Nonhermitian Effects in Linear and Saturable Scattering,” (2020).
49. J. Bechhoefer, “Kramers–Kronig, Bode, and the meaning of zero,” Am. J. Phys. **79**, 1053–1059 (2011).
50. H. M. Nussenzveig, *Causality and Dispersion Relations* (Math.Sci.Eng. 95, Academic Press, New York-London, 1972).
51. H. A. Haus, *Waves and Fields in Optoelectronics.* (Prentice-Hall, New Jersey, 1984).
52. S. Fan, W. Suh, and J. D. Joannopoulos, “Temporal coupled-mode theory for the Fano resonance in optical resonators,” JOSA A **20**, 569–572 (2003).
53. K. X. Wang, Z. Yu, S. Sandhu, and S. Fan, “Fundamental bounds on decay rates in asymmetric single-mode optical resonators,” Opt. Lett. **38**, 100–102 (2013).
54. H. Zhou, B. Zhen, C. W. Hsu, O. D. Miller, S. G. Johnson, J. D. Joannopoulos, and M. Soljacic, “Perfect single-sided radiation and absorption without mirrors,” Optica **3**, 1079–1086 (2016).
55. X. Yin, J. Jin, M. Soljačić, C. Peng, and B. Zhen, “Observation of topologically enabled unidirectional guided resonances,” Nature **580**, 467–471 (2020).
56. G. Liang, H. Huang, A. Mohanty, M. C. Shin, X. Ji, M. J. Carter, S. Shrestha, M. Lipson, and N. Yu, “Robust, efficient, micrometre-scale phase modulators at visible wavelengths,” Nat. Photonics **15**, 908–913 (2021).
57. D. Kim, A. Baucour, Y.-S. Choi, J. Shin, and M.-K. Seo, “Spontaneous generation and active manipulation of real-space optical vortices,” Nature **611**, 48–54 (2022).
58. A. Berkhout and A. F. Koenderink, “Perfect Absorption and Phase Singularities in Plasmon Antenna Array Etalons,” ACS Photonics **6**, 2917–2925 (2019).
59. J. Pomplun, S. Burger, L. Zschiedrich, and F. Schmidt, “Adaptive finite element method for simulation of optical nano structures,” physica status solidi (b) **244**, 3419–3434 (2007).
60. C. Yan, T. V. Raziman, and O. J. F. Martin, “Phase Bifurcation and Zero Reflection in Planar Plasmonic Metasurfaces,” ACS Photonics **4**, 852–860 (2017).
61. R. Barczyk, S. Nechayev, M. A. Butt, G. Leuchs, and P. Banzer, “Vectorial vortex generation and phase singularities upon Brewster reflection,” Phys. Rev. A **99**, 063820 (2019).
62. S. W. D. Lim, J.-S. Park, M. L. Meretska, A. H. Dorrah, and F. Capasso, “Engineering phase and polarization singularity sheets,” Nat. Commun. **12**, 4190 (2021).

63. G. Ermolaev, K. Voronin, D. G. Baranov, V. Kravets, G. Tselikov, Y. Stebunov, D. Yakubovsky, S. Novikov, A. Vyshnevyy, A. Mazitov, I. Kruglov, S. Zhukov, R. Romanov, A. M. Markeev, A. Arsenin, K. S. Novoselov, A. N. Grigorenko, and V. Volkov, "Topological phase singularities in atomically thin high-refractive-index materials," Nat. Commun. **13**, 2049 (2022).
64. M. Elsawy, C. Kyrou, E. Mikheeva, R. Colom, J. Duboz, K. Z. Kamali, S. Lanteri, D. Neshev, and P. Genevet, "Universal Active Metasurfaces for Ultimate Wavefront Molding by Manipulating the Reflection Singularities," Laser & Photonics Rev. p. 2200880 (2023).
65. L. Lin, J. Hu, S. Dagli, J. A. Dionne, and M. Lawrence, "Universal Narrowband Wavefront Shaping with High Quality Factor Meta-Reflect-Arrays," Nano Lett. **23**, 1355–1362 (2023).
66. A. Overvig and A. Alù, "Diffractive Nonlocal Metasurfaces," Laser & Photonics Rev. **16**, 2100633 (2022).
67. R. Chai, Q. Liu, W. Liu, Z. Li, H. Cheng, J. Tian, and S. Chen, "Emerging Planar Nanostructures Involving Both Local and Nonlocal Modes," ACS Photonics (2023).
68. S. Kim, S. Lepeshov, A. Krasnok, and A. Alù, "Beyond Bounds on Light Scattering with Complex Frequency Excitations," Phys. Rev. Lett. **129**, 203601 (2022). Publisher: American Physical Society.

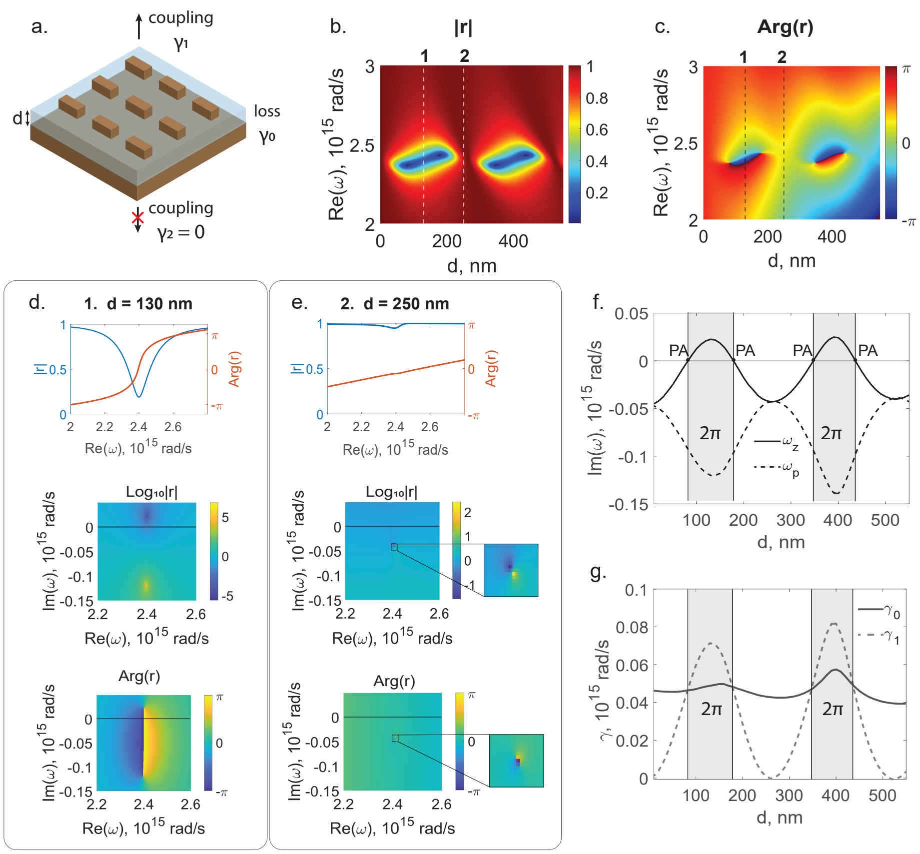

Fig. 2. a. An example of metal-insulator-metal (MIM) metasurface from [58]: the gold mirror is separated from gold resonators by a spacer of thickness d. b. Amplitude and c. The phase of light reflected by the metasurface in (a.) as a function of real frequency and spacer thickness (reproduced from same parameters as in [58]). d. Reflection amplitude and phase maps corresponding to the vertical dashed line denoted by 1 (d = 130 nm in (b.,c.): a 2π resonant phase as a function of the real frequency is obtained. Note that this figure has been plotted using phase unwrap. In the bottom, the logarithm of the reflection amplitude and phase as a function of complex frequency illumination for d = 130 nm. e. Reflection amplitude and the phase maps corresponding to the vertical dashed line denoted by 2 (d = 250 nm in (b.,c.): no resonant phase variation as a function of the real frequency is introduced. In the bottom, the logarithm of the reflection amplitude and phase as a function of complex frequency illumination for d = 250 nm. f. Evolution of the imaginary parts of the complex zeros (ω_{RZ}) and poles (ω_{P}) as a function of the spacer thickness d. Points corresponding to reflection zeros crossing the real axis are noted as PA - perfect absorption. These are the regions where the metasurface produces a resonant phase shift of 2π g. Evolution of the coupling coefficient to the reflection channel γ_1 (dashed line) and the metasurface absorption loss γ_0 (full line) as a function of the spacer thickness d. in f and g, the regions associated with the positive imaginary part of the reflection zero are highlighted with gray.

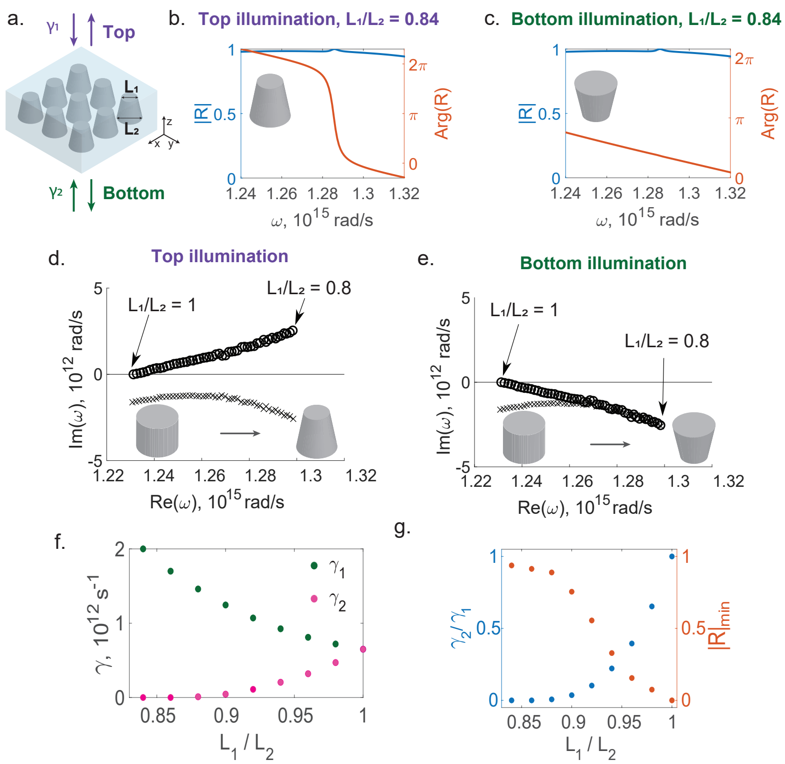

Fig. 3. a. Design of an asymmetric phase-gradient metasurface consisting of a 2D square lattice of conically-shaped silicon meta-atoms embedded in a glass environment. Metasurface can operate almost as a perfect reflector using both top and bottom illumination conditions. b. and c. represent the metasurface reflection amplitude and phase using top and bottom illumination respectively. In b., a resonant 2π phase variation as a function of the excitation frequency is observed. In c., the structure behaves as a simple mirror, without resonant phase variation. d. and e. show the evolution of pole and zero complex plane positions as a function of the asymmetry for top and bottom illumination respectively. We observe that decreasing the asymmetry parameter L_1/L_2 from 1 to 0.8 results in an asymmetric response associated with complex conjugated reflection zeros from the degenerated real frequency symmetric case. f. Coupling coefficients of the top (γ_1) and bottom (γ_2) channels of the metasurface depicted in a. upon top illumination for different out-of-plane asymmetries (L_1/L_2 is changing from 0.8 to 1). g. The ratio between coupling coefficients γ_2/γ_1 and minimum reflection in the selected frequency range shown in b. and c. as functions of L_1/L_2

Supplementary Material

I. TEMPORAL COUPLED MODE THEORY DERIVATIONS

We consider a closed linear system supporting M resonances and interacting with the environment through N external channels. The field amplitudes received and lost by the system are contained in N-dimensional vectors α and β respectively. Incoming and outgoing fields in this system are connected by a scattering matrix $\beta = S(w)\alpha$. To account for the resonant interaction of light with the system, each internal mode can receive or lose energy to the environment from/into the N channels contained in N-dimensional vectors composed of α and β. We study the evolution of this system using the temporal coupled-mode theory (TCMT) [1–3] that describes the resonant scattering of light on the nanoparticles as a superposition of a low quality factor background mode with M high quality factor modes representing the resonant system (Fig. 1a.).

The field coupled to resonances is denoted by an M-dimensional vector **a**, its interaction with incoming and outgoing fields in the channels is described by an $N \times M$ in-coupling matrix K and an out-coupling matrix D, respectively. TCMT connects the outgoing and incoming field with Eqs. 1 that are written considering time-dependence $e^{-i\omega t}$ and assuming time-reversal symmetry implying that the in-coupling and out-coupling coefficients of the system are the same $K = D$. However, according to [3, 4] absorption and gain can still be considered through the non-Hermitian part of H_0 without violating this connection between the coefficients.

$$\begin{cases} -i\omega a = -iH_{CMT}a + D^T\alpha \\ \beta = S_0\alpha + Da \end{cases} \tag{1}$$

Here, a coupled-mode theory Hamiltonian is composed of a closed-system Hamiltonian H_0 and coupling to the environment described with a coupling matrix D: $H_{CMT} \equiv H_0 - i\dfrac{D^\dagger D}{2}$. In TCMT, coupling matrix D is assumed to be frequency-independent, which is not the case for the exact description. However, TCMT still correctly describes many systems, especially when considering comparatively high quality-factor resonances [3, 4]. S_0 is an $N \times N$ direct scattering matrix accounting for the non-resonant background. When one or several high Q-factor resonances are being analyzed in the limited frequency region, the contribution of all the other resonances are summarized by S_0. However, when more resonances are explicitly considered in the model, S_0 approaches a unitary matrix. We further assume it to be a unitary matrix as it doesn't influence the spectral positions of poles and zeros that we aim to retrieve, but for the accurate modeling of the scattering amplitude and phase, this factor should be considered.

Using Eqs. 1,we get the expression for the scattering matrix:

$$S(\omega) = \left(I_N - iD\frac{1}{\omega - H_{CMT}}D^\dagger\right) \tag{2}$$

Considering 2 regions (substrate/superstrate) and dividing all the channels into 2 subsets (Fig. 1b.), we have:

$$D = \begin{bmatrix} D_1 \\ D_2 \end{bmatrix}, D^\dagger = \begin{bmatrix} D_1^\dagger & D_2^\dagger \end{bmatrix} \tag{3}$$

$$S(\omega) = \begin{bmatrix} I_{N_1} - iD_1\dfrac{1}{\omega - H_{CMT}}D_1^\dagger & -iD_1\dfrac{1}{\omega - H_{CMT}}D_2^\dagger \\ -iD_2\dfrac{1}{\omega - H_{CMT}}D_1^\dagger & I_{N_2} - iD_2\dfrac{1}{\omega - H_{CMT}}D_2^\dagger \end{bmatrix} \tag{4}$$

Comparing Eq. 4 with the expression for scattering matrix $S = \begin{bmatrix} r & t' \\ t & r' \end{bmatrix}$ we can write for reflection and transmission coefficients:

$$r = I_{N_1} - iD_1\frac{1}{\omega - H_{CMT}}D_1^\dagger \tag{5}$$

$$t = -iD_2\frac{1}{\omega - H_{CMT}}D_1^\dagger \tag{6}$$

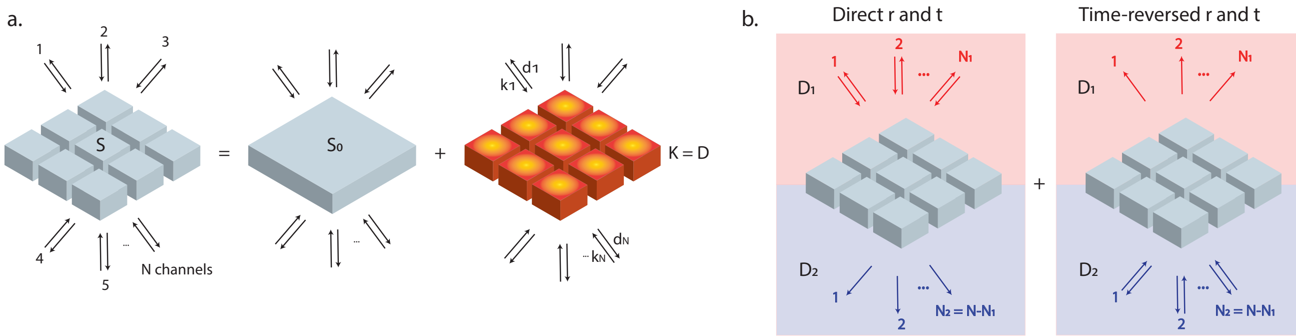

FIG. 1. a. Transient coupled mode theory describes a linear system interacting with environment through N channels. It considers system's response as an interference of non-resonant background including all the low-quality factor contributions and a finite number of high quality factor resonant modes. TCMT quantifies energy exchange between system and environment by introducing in-coupling coefficient K and out-coupling coefficient D

A. Derivation of the analytical expression for reflection zeros and poles

We start derivation from the expression for the reflection matrix Eq. 5:

$$r(\omega) = I_{N_1} - iD_1 \frac{1}{\omega - H_0 + i\frac{D^\dagger D}{2}} D_1^\dagger \tag{7}$$

The total coupling between the system and environment comprises coupling with incoming and outgoing channels: $\frac{D^\dagger D}{2} = \frac{D_1^\dagger D_1}{2} + \frac{D_2^\dagger D_2}{2}$

$$\begin{aligned} r(\omega) = \quad & I_{N_1} - iD_1 \times \\ & \times \left(\omega - H_0 + i\frac{D_1^\dagger D_1}{2} + i\frac{D_2^\dagger D_2}{2}\right)^{-1} D_1^\dagger \end{aligned} \tag{8}$$

Using linear algebra identity $(A + BC)^{-1}B = A^{-1}B(I + CA^{-1}B)^{-1}$, derive

$$\begin{aligned} r(\omega) = \quad & I_{N_1} - \\ & - \frac{iD_1 \left(\omega - H_0 + i\frac{D_2^\dagger D_2}{2}\right)^{-1} D_1^\dagger}{I_{N_1} + i\frac{D_1}{2}\left(\omega - H_0 + i\frac{D_2^\dagger D_2}{2}\right)^{-1} D_1^\dagger} \end{aligned} \tag{9}$$

Writing the previous expression with a common denominator

$$r(\omega) = \frac{I_{N_1} - i\frac{D_1}{2}\left(\omega - H_0 + i\frac{D_2^\dagger D_2}{2}\right)^{-1} D_1^\dagger}{I_{N_1} + i\frac{D_1}{2}\left(\omega - H_0 + i\frac{D_2^\dagger D_2}{2}\right)^{-1} D_1^\dagger} \tag{10}$$

Calculate reflection matrix determinant:

$$\det(r(\omega)) = \frac{\det\left(I_{N_1} - i\frac{D_1}{2}\left(\omega - H_0 + i\frac{D_2^\dagger D_2}{2}\right)^{-1} D_1^\dagger\right)}{\det\left(I_{N_1} + i\frac{D_1}{2}\left(\omega - H_0 + i\frac{D_2^\dagger D_2}{2}\right)^{-1} D_1^\dagger)\right)} \tag{11}$$

Using linear algebra identity $det(I - BC) = det(I - CB)$, derive

$$\det(r(\omega)) = \frac{det\left(\omega - H_0 + i\frac{D_2^\dagger D_2}{2} - i\frac{D_1^\dagger D_1}{2}\right)}{det\left(\omega - H_0 + i\frac{D_2^\dagger D_2}{2} + i\frac{D_1^\dagger D_1}{2})\right)} \tag{12}$$

We can write this expression as

$$\det(r(\omega)) = \frac{det(\omega - H_{RZ})}{det(\omega - H_{CMT})} \tag{13}$$

In $H_{RZ} = H_0 - i\frac{D_2^\dagger D_2}{2} + i\frac{D_1^\dagger D_1}{2}$ coupling to the input channel comes with a plus sign and can be considered as effective gain while coupling to the output channel comes with a minus sign and considered as the effective loss[3].

Condition for reflection zero $\det(r(\omega = \omega_{RZ})) = 0$ is expressed as:

$$\omega_{RZ} = H_0 - i\frac{D_2^\dagger D_2}{2} + i\frac{D_1^\dagger D_1}{2} \tag{14}$$

B. Derivation of the analytical expression for transmission zeros and poles

Expression for the scattering matrix (Eq. 4) shows that, unlike for reflection, equation for transmission matrix (Eq. 15) doesn't contain a unity matrix I_{N_1} as it is off the $S-$matrix main diagonal.

$$t = -iD_2 \frac{1}{\omega - H_0 + \frac{iD_1^\dagger D_1}{2} + \frac{iD_2^\dagger D_2}{2}} D_1^\dagger \tag{15}$$

For this reason, the expression for the determinant of the transmission matrix can not be as easily factorized as the one for the reflection matrix (Eq. 13). Instead, it contains two factors (Eq. 16), and when one of them is equal to zero, another one diverges (please find the detailed derivation below):

$$\det(t) = (-i)^N \frac{\det(\omega - H_0)\det(D_2(\omega - H_0)^{-1}D_1^\dagger)}{\det(\omega - H_{CMT})} \tag{16}$$

However, in [5] it was proven (in a framework of the Heidelberg model), that the numerator in Eq. 16 has to be real in the time-reversal symmetric structure (that doesn't contain absorption loss or gain). In its turn, it implies that transmission zeros in such systems exist only on the real axis or in complex-conjugated pairs which is the case for Huygens metasurfaces combining two modes to reach 2π resonant phase shift. [6]

1. *Derivation for* $\det(T)$

Expression for transmission matrix:

$$t = -iD_2 \frac{1}{\omega - H_{CMT}} D_1^\dagger \tag{17}$$

$$t = -iD_2 \frac{1}{\omega - H_0 + \frac{iD_1^\dagger D_1}{2} + \frac{iD_2^\dagger D_2}{2}} D_1^\dagger \tag{18}$$

Using linear algebra identity $\left(A + BC\right)^{-1} B = A^{-1} B \left(I + CA^{-1}B\right)^{-1}$, derive

$$t = \frac{-iD_2(\omega - H_0 + \frac{iD_2^\dagger D_2}{2})^{-1} D_1^\dagger}{I + i\frac{D_1}{2}(\omega - H_0 + \frac{iD_2^\dagger D_2}{2})^{-1} D_1^\dagger} \tag{19}$$

We calculate the transmission matrix determinant

$$\det(t) = \frac{\det(-iD_2(\omega - H_0 + \frac{iD_2^\dagger D_2}{2})^{-1} D_1^\dagger)}{\det(I + i\frac{D_1}{2}(\omega - H_0 + \frac{iD_2^\dagger D_2}{2})^{-1} D_1^\dagger)} \tag{20}$$

Using linear algebra identity $det\,(I - BC) = det\,(I - CB)$, derive

$$\det(t) = \frac{\det(-iD_2(\omega - H_0 + \frac{iD_2^\dagger D_2}{2})^{-1} D_1^\dagger)}{\det(I + \frac{iD_1^\dagger D_1}{2}(\omega - H_0 + \frac{iD_2^\dagger D_2}{2})^{-1})} \tag{21}$$

which transforms into

$$\det(t) = \frac{\det(\omega - H_0 + \frac{iD_2^\dagger D_2}{2})\det(-iD_2(\omega - H_0 + \frac{iD_2^\dagger D_2}{2})^{-1} D_1^\dagger)}{\det(\omega - H_0 + \frac{iD_2^\dagger D_2}{2} + \frac{iD_1^\dagger D_1}{2})} \tag{22}$$

While the denominator in this expression is the same as for reflection and scattering, the numerator consists of two terms and doesn't allow to derive a simple rule for transmission zeros, as it was done for reflection.

$$\det(t) = \frac{\det(\omega - H_0 + \frac{iD_2^\dagger D_2}{2})\det(-iD_2(\omega - H_0 + \frac{iD_2^\dagger D_2}{2})^{-1} D_1^\dagger)}{\det(\omega - H_{CMT})} \tag{23}$$

$$\det(t) = \frac{\det(\omega - H_0)\det(I + (\omega - H_0)^{-1}\frac{iD_2^\dagger D_2}{2})\det(-iD_2(\omega - H_0 + \frac{iD_2^\dagger D_2}{2})^{-1} D_1^\dagger)}{\det(\omega - H_{CMT})} \tag{24}$$

$$\det(t) = \frac{\det(\omega - H_0)\det(I + \frac{iD_2}{2}(\omega - H_0)^{-1} D_2^\dagger)\det(-iD_2(\omega - H_0 + \frac{iD_2^\dagger D_2}{2})^{-1} D_1^\dagger)}{\det(\omega - H_{CMT})} \tag{25}$$

$$\det(t) = \frac{\det(\omega - H_0)\det(-iI)\det(D_2(I + \frac{i}{2}(\omega - H_0)^{-1} D_2^\dagger D_2)(\omega - H_0 + \frac{iD_2^\dagger D_2}{2})^{-1} D_1^\dagger}{\det(\omega - H_{CMT})} \tag{26}$$

$$\det(t) = (-i)^N \frac{\det(\omega - H_0)\det(D_2(I + \frac{i}{2}(\omega - H_0)^{-1}D_2^\dagger D_2)(\omega - H_0)^{-1}(I + \frac{i}{2}(\omega - H_0)^{-1}D_2^\dagger D_2)^{-1}D_1^\dagger)}{\det(\omega - H_{CMT})} \tag{27}$$

$$\det(t) = (-i)^N \frac{\det(\omega - H_0)\det(D_2(\omega - H_0)^{-1}D_1^\dagger)}{\det(\omega - H_{CMT})} \tag{28}$$

II. ASYMMETRIC SILICON STRUCTURE

In order to obtain a full 2π resonant phase gradient in reflection, we design a lossless silicon-based metasurface ($n = 3.5$). Starting from silicon cylinders with the height $h = 600$ nm arranged in a 2D square lattice with a fixed period of $p = 800$ nm, we induce the asymmetry by reducing the top diameter of the cylinder creating truncated cones. We also embed the interface into a homogeneous medium with a refractive index $n = 1.5$. When the pillar shape is preserved, i.e. when their top and bottom diameters defined as L_1 and L_2 respectively are equal ($L_1 = L_2$), the zeros are fixed to the real axis, while when L_1 and L_2 are different, the zero has a complex value. Figure 2 shows how the reflection phase and amplitude are changing with a gradual change of diameters ratio from $L_1/L_2 = 1$ to $L_1/L_2 = 0.8$ in a case of top illumination ($L_2 = 500nm$). The amplitude map shows a gradual increase of reflection with increasing asymmetry. We add to it the reflection amplitude calculated in a complex frequency plane for $L_1/L_2 = 1$ (reflection zero is indeed on the real axis because of coupling symmetry) and $L_1/L_2 = 0.84$ (reflection zero is almost a complex-conjugate of pole which is a condition for maximum reflection amplitude). For all the range of chosen values except $L_1/L_2 = 1$ the designed metasurface demonstrates a sharp resonant 2π jump. The phase maps also calculated in the complex plane for the same parameters show that for $L_1/L_2 = 1$ the branch cut connecting pole and zero only touches the real axis resulting in a π phase jump, while for $L_1/L_2 = 0.84$ the branch cut crosses the real axis which results in a 2π phase gradient.

[1] S. Fan, W. Suh, and J. D. Joannopoulos, Temporal coupled-mode theory for the Fano resonance in optical resonators, JOSA A **20**, 569 (2003).

[2] F. Alpeggiani, N. Parappurath, E. Verhagen, and L. Kuipers, Quasinormal-Mode Expansion of the Scattering Matrix, Physical Review X **7**, 021035 (2017).

[3] W. R. Sweeney, Electromagnetic Eigenvalue Problems and Nonhermitian Effects in Linear and Saturable Scattering (2020).

[4] W. R. Sweeney, C. W. Hsu, and A. D. Stone, Theory of reflectionless scattering modes, Physical Review A **102**, 063511 (2020), publisher: American Physical Society.

[5] Y. Kang and A. Z. Genack, Transmission zeros with topological symmetry in complex systems, Physical Review B **103**, L100201 (2021).

[6] R. Colom, E. Mikheeva, K. Achouri, J. Zuniga-Perez, N. Bonod, O. J. F. Martin, S. Burger, and P. Genevet, Crossing of the Branch Cut: The Topological Origin of a Universal 2π-Phase Retardation in Non-Hermitian Metasurfaces, Laser & Photonics Reviews , 2200976 (2023).

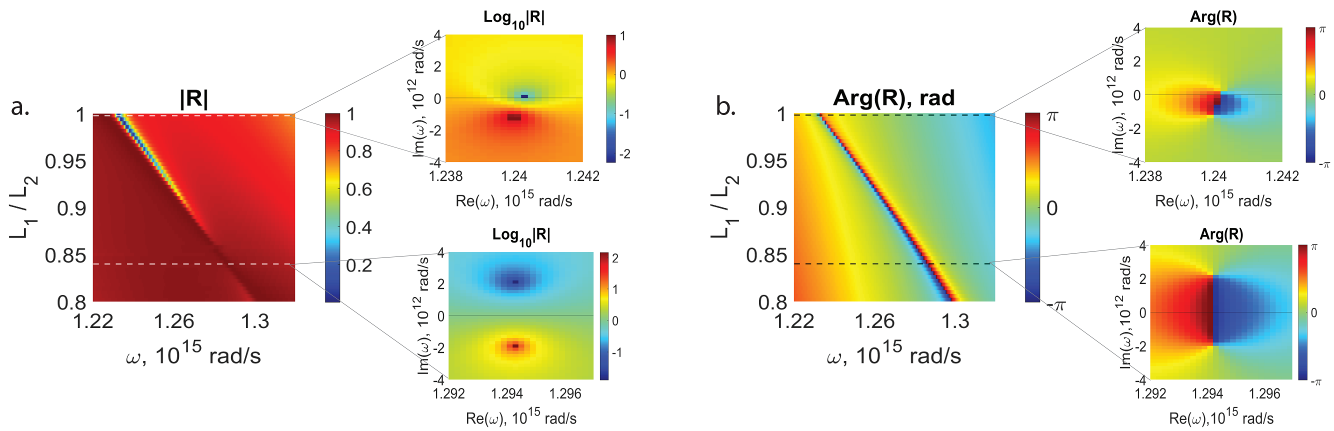

FIG. 2. a. Reflection amplitude as a function of real frequency and the ratio of the top and bottom diameters of truncated silicon cones composing a metasurface. on the right, reflection amplitude in a complex frequency plane for 2 asymmetry values $L_1/L_2 = 1$ and $L_1/L_2 = 0.84$. b. Reflection phase as a function of real frequency and the diameters ratio L_1/L_2. On the right, reflection phase in a complex frequency plane for 2 asymmetry values $L_1/L_2 = 1$ and $L_1/L_2 = 0.84$.